AJNR

Cerebral Aneurysms Treated with Flow-Diverting Stents: Computational Models with Intravascular Blood Flow Measurements

M.R. Levitt, P.M. McGah, A. Aliseda, P.D. Mourad, J.D. Nerva, S.S. Vaidya, R.P. Morton, B.V. Ghodke and L.J. Kim

AJNR Am J Neuroradiol published online 18 July 2013
http://www.ajnr.org/content/early/2013/07/18/ajnr.A3624

Published July 18, 2013 as 10.3174/ajnr.A3624

Cerebral Aneurysms Treated with Flow-Diverting Stents: Computational Models with Intravascular Blood Flow Measurements

M.R. Levitt, P.M. McGah, A. Aliseda, P.D. Mourad, J.D. Nerva, S.S. Vaidya, R.P. Morton, B.V. Ghodke, and L.J. Kim

ABSTRACT

BACKGROUND AND PURPOSE: Computational fluid dynamics modeling is useful in the study of the hemodynamic environment of cerebral aneurysms, but patient-specific measurements of boundary conditions, such as blood flow velocity and pressure, have not been previously applied to the study of flow-diverting stents. We integrated patient-specific intravascular blood flow velocity and pressure measurements into computational models of aneurysms before and after treatment with flow-diverting stents to determine stent effects on aneurysm hemodynamics.

MATERIALS AND METHODS: Blood flow velocity and pressure were measured in peri-aneurysmal locations by use of an intravascular dual-sensor pressure and Doppler velocity guidewire before and after flow-diverting stent treatment of 4 unruptured cerebral aneurysms. These measurements defined inflow and outflow boundary conditions for computational models. Intra-aneurysmal flow rates, wall shear stress, and wall shear stress gradient were calculated.

RESULTS: Measurements of inflow velocity and outflow pressure were successful in all 4 patients. Computational models incorporating these measurements demonstrated significant reductions in intra-aneurysmal wall shear stress and wall shear stress gradient and a trend in reduced intra-aneurysmal blood flow.

CONCLUSIONS: Integration of intravascular dual-sensor guidewire measurements of blood flow velocity and blood pressure provided patient-specific computational models of cerebral aneurysms. Aneurysm treatment with flow-diverting stents reduces blood flow and hemodynamic shear stress in the aneurysm dome.

ABBREVIATIONS: CFD = computational fluid dynamics; WSS = wall shear stress; WSSG = wall shear stress gradient; TCD = transcranial Doppler ultrasonography; pcMRA = phase-contrast MRA

Flow-diverting stent technology[1] is thought to reduce blood flow (and hence hemodynamic stresses) inside cerebral aneurysms, promoting thrombosis and lowering rupture risk.[2] However, 15–35% of aneurysms treated with flow-diverting stents remain patent at midterm angiographic follow-up.[3-6] Risk factors for persistent aneurysm patency include previous aneurysm treatment and female sex, though accurate predictors of treatment failure and delayed hemorrhagic complications have not been completely elucidated.[7-9]

Computational fluid dynamics (CFD) modeling of aneurysms and the surrounding cerebral vasculature allows investigators to study important hemodynamic characteristics such as wall shear stress (WSS)[10,11] and wall shear stress gradient (WSSG),[12] which have been implicated in aneurysm growth, rupture, and treatment failure.[13] Recently, CFD analysis has been applied to the effects of flow-diverting stent treatment in an attempt to understand how flow diversion affects aneurysm hemodynamics for both treatment success[14] and complication avoidance.[15-17] However, these reports did not use patient-specific measurements of blood flow velocity and blood pressure when creating CFD models, which may have affected their results.[18,19]

Received February 26, 2013; accepted after revision April 14.

From the Departments of Neurological Surgery (M.R.L., P.D.M., J.D.N., R.P.M., B.V.G., L.J.K.), Mechanical Engineering (P.M.M., A.A.), Applied Physics Laboratory (P.D.M.), Bioengineering (P.D.M.), and Radiology (P.D.M., S.S.V., B.V.G., L.J.K.), University of Washington, Seattle.

This work was supported by NINDS/NIH grant R03NS078539, and in part by US Army Medical Research and Material Command contract No. W81XWH-11–1-0109, an unrestricted grant from Volcano Corporation, San Diego, California, and the generous support of Mark Robison and family.

Paper previously presented as an abstract at: American Society of Mechanical Engineering 2013 Summer Bioengineering Conference, June 26–29, 2013, Sun River, Oregon.

Please address correspondence to Louis J. Kim, MD, Box 359924, Department of Neurological Surgery, Harborview Medical Center, 325 9th Ave, Seattle, WA 98104; e-mail: ljkim1@u.washington.edu

Indicates open access to non-subscribers at www.ajnr.org

Indicates article with supplemental on-line appendix.

Indicates article with supplemental on-line figures.

http://dx.doi.org/10.3174/ajnr.A3624

We incorporated patient-specific measurements of blood flow velocity and blood pressure in the peri-aneurysmal environment into the boundary conditions of CFD to determine the hemodynamic effects of flow-diverting stents on unruptured aneurysms.

MATERIALS AND METHODS

Population

Four patients with unruptured cerebral aneurysms were included in this institutional review board–approved prospective study, and informed consent was obtained. Patient, aneurysm, anatomic, and device characteristics are shown in On-line Table 1. All patients underwent endovascular flow-diverting stent placement by use of the Pipeline Embolization Device (Covidien/ev3, Irvine, California) under isofluorane inhalational anesthesia. The aneurysm in patient 1 was also partially coiled. Patient temperature, hematocrit, and end-tidal CO_2 were recorded. Three-dimensional rotational angiography was obtained before aneurysm treatment, and contrast-enhanced flat panel CT was obtained after treatment for stent visualization.[20]

Patient-Specific Data Collection

Blood flow velocity and blood pressure were measured by use of the dual-sensor pressure and Doppler velocity guidewire (ComboWire, Volcano Corporation, Rancho Cordova, California) and workstation (ComboMap, Volcano). The tip of the 0.014-inch wire contains a piezoresistive pressure sensor and piezoelectrode Doppler device that emits a 45° sonography beam that measures velocity 5 mm beyond the tip. This wire has been used to measure patient-specific blood pressure and blood flow velocity in both coronary[21] and cerebral vessels,[22,23] with excellent anatomic specificity and correlation to measured blood flow.[24] In the current study, pressure and velocity were sampled every 5 ms, and peak systolic, diastolic, and average pressures and velocities were calculated automatically by the workstation on the basis of the cardiac cycle.

Before aneurysm treatment, the dual-sensor guidewire was placed in 2 predetermined peri-aneurysmal locations: 1) proximal petrous carotid artery, and 2) 5 mm distal to the aneurysm neck. The wire was oriented along the long axis of vessel flow to maximize the flow velocity signal, and radiographs of the location of the wire were obtained. Blood pressure and blood flow velocity were recorded for at least 10 cardiac cycles at each location before wire removal. After aneurysm treatment, the wire was reintroduced and the same measurements were taken again at all locations. Effort was made to reproduce the exact wire locations during pretreatment measurements as recorded in previous radiographs. Blood pressure and blood flow velocity measurements were exported to a workstation for CFD analysis.

Computational Modeling

Three-dimensional reconstructions of the vessels were created from the rotational angiographic images by use of the Vascular Modeling Toolkit (Bergamo, Italy; www.vmtk.org). Ophthalmic and posterior communicating arteries and other small side-branching vessels were eliminated from each model, except for the posterior communicating artery in patient 1 because they had a negligible effect on hemodynamic calculations (On-line Appendix). A "virtual stent" was placed into each reconstruction for posttreatment simulations by inserting a saddle-shaped surface to the location of the stent boundary on the basis of its location in the posttreatment CT. The stent was modeled as a thin, porous surface with specified pressure-loss coefficients, taken from a previous study[25] that computed the pressure drops over low-porosity flow-diverting stents. Pressure drops were parameterized as 2 unique loss coefficients integrated into our CFD model (On-line Appendix). In patient 1 (in whom the aneurysm was partially coiled), a shear and shear gradient value of zero was assigned to the area of the aneurysm dome excluded after coiling, and the remaining volume was used for hemodynamic calculations. Tetrahedral meshes were generated for all simulations by use of the ANSYS Gambit package, release 2.4 (ANSYS, Canonsburg, Pennsylvania). The characteristic width of the computational mesh cells was 0.2 mm for all cases. Simulations were executed by use of ANSYS Fluent, release 12.1 (ANSYS), a finite-volume-based solver. The blood was assumed to be incompressible and Newtonian, with an attenuation of 1050 kg/m^3 and viscosity of 3.5 cP.

At the proximal vessel, the time-dependent Womersley velocity profile was prescribed by use of velocity measurements from the dual-sensor guidewire at position 1 (petrous carotid artery). These measured velocities were matched to the centerline velocity of the Womersley flow and used as inflow conditions, incorporating the cross-sectional vessel area from the pretreatment and posttreatment 3D vessel reconstructions (Fig 1, On-line Appendix). At distal vessels, pressures were prescribed by use of measurements from the dual-sensor guidewire at position 2 (5 mm distal to the aneurysm neck) for use as outflow conditions. Velocity and pressure waveforms were phase-averaged over at least 10 cardiac cycles before CFD modeling. Flow rates were computed directly from the wire-derived Womersley velocity profile. Slight changes in heart rate, mean arterial pressure, and blood flow after treatment were incorporated into posttreatment CFD models. The CFD simulations were computed over 3 cardiac cycles, and the first 2 cycles were excluded from analysis to ensure that the simulation was independent of the initializing condition. Intra-aneurysmal blood flow, WSS, and WSSG were calculated over the entire aneurysm volume in each patient (On-line Appendix). Flow rates, WSS, and WSSG were determined both at the moment of peak systole and averaged over an entire cardiac cycle. Pressure drops were also simulated between the 2 wire locations (petrous carotid artery and 5 mm distal to the aneurysm neck), without patient-specific guidewire-derived pressure values. Statistical comparisons were made by use of the Student *t* test.

RESULTS

Patient-Specific Measurements

Proximal blood flow velocity and distal blood pressure measurements were successful in all 4 patients both before and after treatment. Blood flow velocity and flow rates at position 1 (petrous carotid, used for inflow velocity boundary conditions) are shown in Table 1. Flow rates are presented both as an average over the entire cardiac cycle and at the moment of peak systole. The differences between pretreatment and posttreatment velocity and blood flow (both average and peak systolic) at the petrous carotid artery were not significant ($P > .17$).

Table 1: Dual-sensor guidewire measurements of peak systolic blood flow velocity and flow rate used for inflow boundary conditions

n	Blood Flow Velocity, cm/s		Flow Rate, mL/min: Averaged Over Cardiac Cycle		Flow Rate, mL/min: At Peak Systole	
	Pre	Post	Pre	Post	Pre	Post
1	46.92	47.11	165.45	154.83	328.88	236.36
2	37.18	37.28	101.92	110.04	147.52	156.28
3	42.05	46.3	137.20	149.09	209.78	239.12
4	48.17	53.37	170.240	191.02	269.69	311.23
Average	43.58	46.02	143.70	151.25	238.97	235.75
Standard deviation	5.02	6.63	31.44	33.15	77.98	63.31
P		.17		.34		.92

Note:—Pre indicates pretreatment; post, posttreatment.

Complications
There were no intraprocedural or periprocedural complications associated with the use of the dual-sensor guidewire. No vascular injury, thromboembolic event, or new neurologic deficit was observed in any patient.

Computational Modeling
Modeling of WSS and WSSG is shown for each patient in Fig 1. Colorized maps of the top row of each panel demonstrate pretreatment conditions, the middle row shows posttreatment, and the bottom row shows the effect of treatment, as calculated by the difference between pretreatment and posttreatment. In patient 1, after flow diversion and partial coiling, both WSS and WSSG were reduced at the aneurysm neck and impact area of the wall opposite the inflow zone (Fig 1*A*). In patient 2, the sidewall aneurysm demonstrated similar findings of WSS and WSSG reduction in the neck and impact area, with corresponding increase in the downstream parent vessel (Fig 1*B*). Modeling of patient 3, with a more spherical aneurysm, showed reduction in WSS in nearly the entirety of the aneurysm dome and neck and a slight increase in WSSG in the neck midpoint (Fig 1*C*). WSS and WSSG were reduced in the small sidewall aneurysm of patient 4, with increases in these parameters in the surrounding parent vessel (Fig 1*D*).

The wire-based CFD calculations of the effects of flow-diverting stent treatment on intra-aneurysmal hemodynamics are shown in Table 2. Reduction of all parameters was observed in all patients, with significant decreases in WSS and peak-systolic WSSG and trends in reduced blood flow ($P = .07$) and cardiac cycle–averaged WSSG ($P = .06$). Simulated pressure drops across the entire CFD model are shown in On-line Table 2. The average and peak-systolic change in pressure drop after treatment were -0.09 ± 0.26 mm Hg and -0.85 ± 2.08 mm Hg, respectively. The differences were not significant ($P = .55$ and .47).

DISCUSSION
We have successfully incorporated patient-specific measurements of blood flow velocity and blood pressure into CFD modeling of unruptured cerebral aneurysms before and after treatment with flow-diverting stents. The method of applying patient-specific boundary conditions to CFD modeling and quantifying the effects of flow-diverting stents on aneurysmal hemodynamics has not been previously reported. This method may improve the ability of CFD to determine hemodynamic factors associated with treatment, including aneurysm occlusion, persistent patency, or delayed hemorrhagic complications.

The premise of aneurysmal flow diversion is the reduction of blood flow into the aneurysm dome, promoting intra-aneurysmal thrombosis and promoting endothelialization of the stent wall, which reconstructs the parent vessel excluding the aneurysm. Reduction of hemodynamic stress is thought to be crucial in achieving this goal, and the determination of such stress is a key application of CFD analysis.[14] We observed a reduction of flow rate, WSS, and WSSG in the aneurysmal domes. Previous reports of CFD modeling for aneurysmal flow diversion have shown similar reductions in intra-aneurysmal velocity and WSS, though WSSG has not been consistently described.[2,14,17] We also observed a (nonsignificant) increase in blood flow in the parent vessel after treatment, possibly the result of the exclusionary effect of flow diversion on aneurysmal blood capacitance.

Increased pressure within the aneurysm dome has been suggested as a possible mechanism for delayed aneurysm rupture after flow-diverting stent treatment. However, in the current study, blood pressure measurements in peri-aneurysmal locations did not change substantially after aneurysm treatment, nor did simulated pressure drops. This is in contrast to a previous CFD report of large pressure drops[16] and increased mural tension[17] after flow diversion but similar to previous CFD[26,27] and in vivo[28] intra-aneurysmal pressure measurements that did not demonstrate changes after flow-diverting stent treatment. Although we did not measure pressure within the aneurysm lumen directly, it is unlikely that a substantial intraluminal increase occurred in the face of such small pressure drops, especially considering the lack of preaneurysmal stenosis in the aneurysms we studied.

Average peak inflow velocity in the petrous carotid artery pretreatment and posttreatment was 43.58 cm/s and 46.02 cm/s, respectively, with a mean flow rate of 143.70 mL/min. Studies of sonography[29] and phase-contrast MRA (pcMRA)[30] velocities of healthy volunteers showed average flow rates of 234 and 277 mL/min, respectively. The use of idealized assumptions of blood flow velocity and blood pressure (rather than patient-specific measurements) as boundary conditions would have significantly affected the results of our hemodynamic calculations.[18,31,32] The origin of our lower flow rate values is unclear; however, healthy volunteers in studies of reference velocity were younger than our patients (average age, 28 ± 7 years). Age is inversely correlated to the measured flow rate in the cerebral vasculature in some studies[33] but not in others.[34] However, we are confident that our direct physiologic measurements with the use of the dual-sensor guidewire were accurate when measuring such parameters in vivo, as shown in animal studies comparing such measurements with direct measurements of blood flow.[24]

Efforts to improve the accuracy of CFD for better applicability to an individual patient's treatment have led to the incorporation of patient-specific blood flow measurements derived from trans-

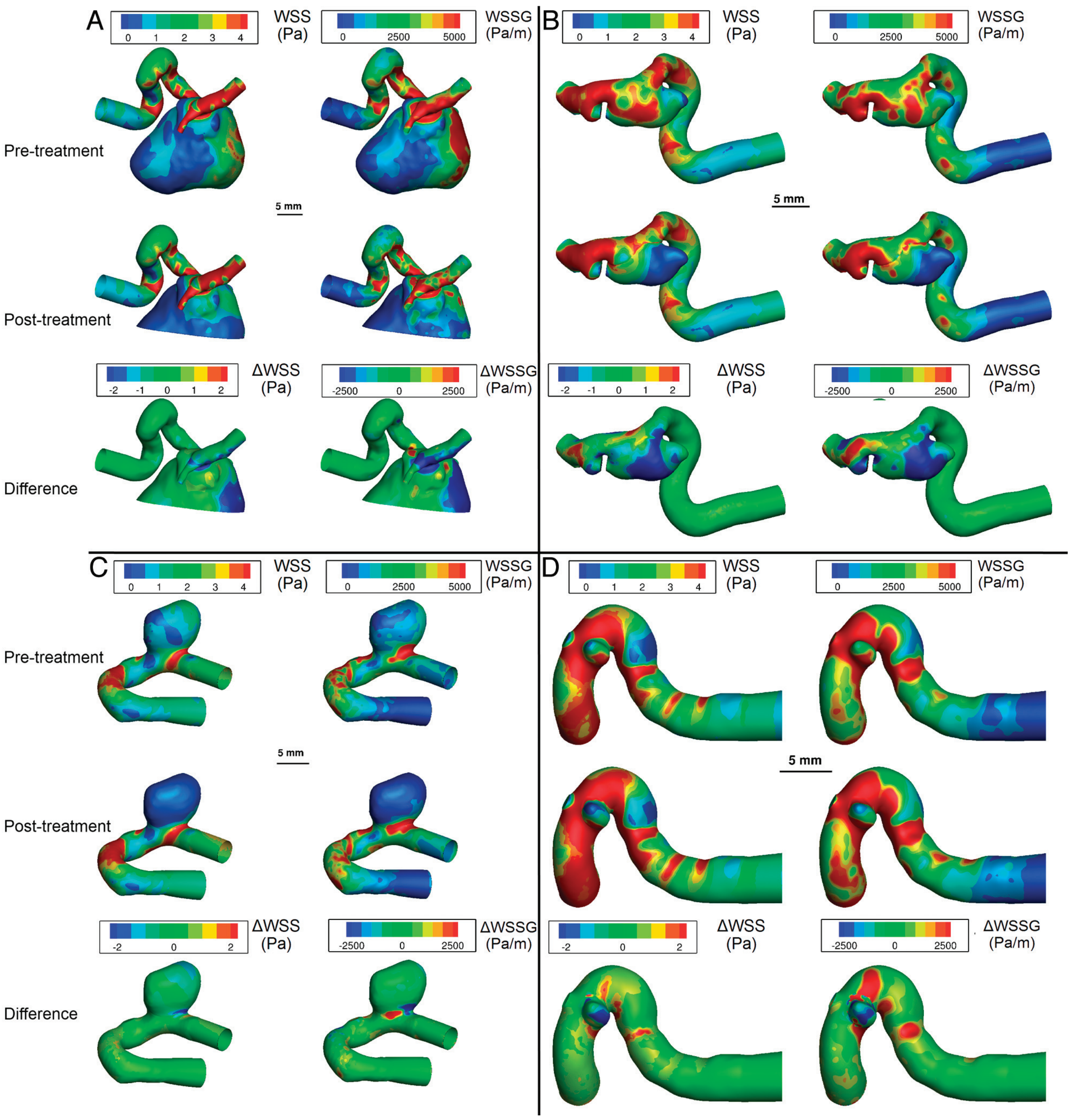

FIG 1. Computational models of 4 aneurysms (*A–D*) integrating patient-specific dual-sensor guidewire measurements of blood flow velocity and pressure. Wall shear stress and wall shear stress gradient are shown before and after treatment (top and middle rows, respectively). The difference (bottom row) represents the effect of treatment on WSS (ΔWSS) and WSSG (ΔWSSG).

Table 2: Computational model-based calculations of intra-aneurysmal hemodynamics before and after flow-diversion treatment with the use of patient-specific boundary conditions from the dual-sensor guidewire

Measure		Pretreatment	Posttreatment	% Change	*P*
Blood flow, mL/min	Time-averaged	81.36	51.38	−39.33%	.07
	Peak systolic	123.25	88.28	−28.84%	.07
WSS, Pa	Time-averaged	1.99	0.92	−56.77%	.03
	Peak systolic	3.92	2.20	−51.89%	.01
WSSG, Pa/m	Time-averaged	2807.95	1730.70	−43.38%	.06
	Peak systolic	6261.35	4236.05	−42.93%	.04

cranial Doppler ultrasonography (TCD)[35,36] or pcMRA[37-39] as input conditions. Acquiring flow rates by use of TCD is fast and noninvasive but may not be accurate in the vertebrobasilar system[40] or in small-caliber vessels or in those near the skull base[41] and cannot be obtained in up to 16% of patients lacking adequate temporal bone windows.[42] When compared with TCD[43] and traditional CFD,[44] flow rates acquired with pcMRA have a lower temporal resolution and may underestimate peak velocity by up to 30%, especially in smaller-diameter vessels.[44] This degree of error may substantially influence WSS results.[18,44] Additionally, pcMRA velocity data must be acquired outside of the angiographic workflow, are both time-consuming and expensive to acquire, and require transport that may be dangerous in critically ill patients.[45] These disadvantages reduce the utility of pcMRA- and TCD-derived flow velocities.

The dual-sensor guidewire has several advantages over the above techniques in acquiring patient-specific measurements. Unlike TCD, it can be used in a highly anatomically specific manner in any major blood vessel, including in the vertebrobasilar system, and does not require temporal bone windows. Advantages over pcMRA include the real-time integration of blood flow velocity measurements during angiography, without transport to and from MR imaging. In addition, a previous report of direct comparison between blood flow velocity measured by pcMRA and the dual-sensor guidewire showed that pcMRA underestimated peak systolic velocity, which could alter CFD-derived hemodynamic calculations.[23] Finally, neither TCD nor pcMRA acquire blood pressure measurements, whereas the dual-sensor nature of the guidewire allows additional integration of this physiologic parameter into CFD modeling. To our knowledge, the incorporation of pressure change data into boundary condition calculations for aneurysmal CFD modeling has not been previously reported. Application of this technique in follow-up studies may help to determine hemodynamic factors responsible for success or failure of flow-diverting stent treatment.

This study has several limitations. First, a small number of patients were studied with variable aneurysmal size and morphology, reducing the study's generalizability (though aneurysm location, vessel diameter, measured velocity, and waveform morphology were similar among all 4 studied patients). Second, although we attempted to recreate the exact location of the dual-sensor guidewire in pretreatment and posttreatment conditions, small variations in the location or angle of the wire may have influenced blood pressure and velocity measurements. Third, the position of the virtual stent in posttreatment CFD and the CFD-derived velocities may not precisely match their in vivo locations. These localization errors were minimized by use of multiple-projection radiographs and 3D volumes to plan virtual wire and stent placement. Fourth, changes in patient systemic hemodynamic status over the course of treatment may have influenced velocity and pressure measurements through the variance of systemic blood pressure, temperature, and end-tidal CO_2. Fifth, subtle changes in stent porosity caused by deformity in curved cerebral vessels was not incorporated into CFD simulations.[15] Finally, though the wire was manipulated in an attempt to measure the most robust velocity signal, it is possible that the measured blood flow velocity was not perfectly aligned within the center of the vessel, resulting in slight underestimations or error in these measurements.[46]

CONCLUSIONS

We have successfully incorporated dual-sensor guidewire measurements of blood pressure and blood flow velocity into patient-specific CFD analyses of unruptured cerebral aneurysms before and after flow-diverting stent treatment. In accordance with the therapeutic intent of flow-diverting stents, significant intra-aneurysmal reductions in WSS and WSSG and a trend in reduced blood flow were observed after treatment.

ICMJE DISCLOSURES: Michael Levitt—*RELATED: Grant:* 1) National Institutes of Health/National Institute of Neurological Disease and Stroke,* 2) Volcano Corporation,* Comments: 1) In the form of grant 1R03NS078539 (Co-investigator), 2) In the form of an unrestricted grant without influence on study design, data collection or interpretation, or manuscript editing (Co-investigator); *OTHER RELATIONSHIPS:* This study was supported by the manufacturer of the dual-sensor Doppler guidewire (Volcano Corporation) through a grant made to the Departments of Neurological Surgery and Radiology, University of Washington. The sponsor was shown the final manuscript but had no role in the study design, data collection, data analyses or interpretation. Patrick McGah—*RELATED: Grant:* NIH-NINDS,* Comments: R03 grant to support the research. Alberto Aliseda—*RELATED: Grant:* National Institutes of Health,* Comments: R03 from NINDS. Sandeep Vaidya—*RELATED: Grant:* Volcano.* Basavaraj Ghodke—*RELATED:* 1) NIH/NINDS,* 2) Volcano Corporation,* Comments: 1) Institutional grant 1R03NS078539 (co-investigator) and 2) Clinical study idea (co-principle investigator); *UNRELATED: Other:* Covidien/ev3, Comments: Proctor, under $5000; *OTHER RELATIONSHIPS:* This study was supported by the manufacturer of the dual-sensor Doppler guidewire (Volcano Corporation) through a grant made to the departments of Neurological Surgery and Radiology, University of Washington. The sponsor was shown the final manuscript but had no role in the study design, data collection, data analyses or interpretation. Louis Kim—*RELATED: Grant:* NIH RO3 grant,* Mark Robison private donation grant,* Comments: I am PI on this NIH grant that primarily funded the work in this report. I received a private sector donation from Mark Robison explicitly used for cerebrovascular research. These funds partly funded equipment costs for this study; *Other:* Volcano Inc research grant,* Comments: I am co-PI of this privately funded grant that contributed to equipment and personnel costs; *UNRELATED: Consultancy:* Aesculap, Comments: Consultant neurosurgeon for this medical device company; *Grants/Grants Pending:* Department of Defense grant on surgical robotics*; *Stock/Stock Options:* Spi Surgical, Comments: Early-stage surgical robotics company, co-founder and shareholder (**money paid to institution*).

REFERENCES

1. Lylyk P, Miranda C, Ceratto R, et al. **Curative endovascular reconstruction of cerebral aneurysms with the Pipeline embolization device: the Buenos Aires experience.** *Neurosurgery* 2009;64:632–42
2. Zhang Y, Chong W, Qian Y. **Investigation of intracranial aneurysm hemodynamics following flow diverter stent treatment.** *Med Eng Phys* August 8, 2012 [Epub ahead of print]
3. McAuliffe W, Wycoco V, Rice H, et al. **Immediate and midterm results following treatment of unruptured intracranial aneurysms with the Pipeline embolization device.** *AJNR Am J Neuroradiol* 2012;33:164–70
4. O'Kelly CJ, Spears J, Chow M, et al. **Canadian experience with the Pipeline embolization device for repair of unruptured intracranial aneurysms.** *AJNR Am J Neuroradiol* 2013;34:381–87
5. Piano M, Valvassori L, Quilici L, et al. **Midterm and long-term follow-up of cerebral aneurysms treated with flow diverter devices: a single-center experience.** *J Neurosurg* 2013;118:408–16
6. Yu SC, Kwok CK, Cheng PW, et al. **Intracranial aneurysms: midterm outcome of Pipeline embolization device: a prospective study in 143 patients with 178 aneurysms.** *Radiology* 2012;265:893–901
7. Hampton T, Walsh D, Tolias C, et al. **Mural destabilization after aneurysm treatment with a flow-diverting device: a report of two cases.** *J Neurointerv Surg* 2011;3:167–71
8. Velat GJ, Fargen KM, Lawson MF, et al. **Delayed intraparenchymal hemorrhage following Pipeline embolization device treatment for a giant recanalized ophthalmic aneurysm.** *J Neurointerv Surg* 2012; 4:e24
9. Kulcsar Z, Houdart E, Bonafe A, et al. **Intra-aneurysmal thrombosis as a possible cause of delayed aneurysm rupture after flow-diversion treatment.** *AJNR Am J Neuroradiol* 2011;32:20–25
10. Shojima M, Oshima M, Takagi K, et al. **Magnitude and role of wall shear stress on cerebral aneurysm: computational fluid dynamic study of 20 middle cerebral artery aneurysms.** *Stroke* 2004; 35:2500–05

11. Miura Y, Ishida F, Umeda Y, et al. **Low wall shear stress is independently associated with the rupture status of middle cerebral artery aneurysms.** *Stroke* 2013;44:519–21
12. Meng H, Wang Z, Hoi Y, et al. **Complex hemodynamics at the apex of an arterial bifurcation induces vascular remodeling resembling cerebral aneurysm initiation.** *Stroke* 2007;38:1924–31
13. Li C, Wang S, Chen J, et al. **Influence of hemodynamics on recanalization of totally occluded intracranial aneurysms: a patient-specific computational fluid dynamic simulation study.** *J Neurosurg* 2012;117:276–83
14. Kulcsar Z, Augsburger L, Reymond P, et al. **Flow diversion treatment: intra-aneurismal blood flow velocity and WSS reduction are parameters to predict aneurysm thrombosis.** *Acta Neurochir (Wien)* 2012;154:1827–34
15. Mut F, Cebral JR. **Effects of flow-diverting device oversizing on hemodynamics alteration in cerebral aneurysms.** *AJNR Am J Neuroradiol* 2012;33:2010–16
16. Cebral JR, Mut F, Raschi M, et al. **Aneurysm rupture following treatment with flow-diverting stents: computational hemodynamics analysis of treatment.** *AJNR Am J Neuroradiol* 2011;32:27–33
17. Hassan T, Ahmed YM, Hassan AA. **The adverse effects of flow-diverter stent-like devices on the flow pattern of saccular intracranial aneurysm models: computational fluid dynamics study.** *Acta Neurochir (Wien)* 2011;153:1633–40
18. Venugopal P, Valentino D, Schmitt H, et al. **Sensitivity of patient-specific numerical simulation of cerebral aneurysm hemodynamics to inflow boundary conditions.** *J Neurosurg* 2007;106:1051–60
19. Marzo A, Singh P, Larrabide I, et al. **Computational hemodynamics in cerebral aneurysms: the effects of modeled versus measured boundary conditions.** *Ann Biomed Eng* 2011;39:884–96
20. Levitt MR, Cooke DL, Ghodke BV, et al. **"Stent view" flat-detector CT and stent-assisted treatment strategies for complex intracranial aneurysms.** *World Neurosurg* 2011;75:275–78
21. Bach RG, Kern MJ. **Practical coronary physiology: clinical application of the Doppler flow velocity guide wire.** *Cardiol Clin* 1997;15:77–99
22. Ferns SP, Schneiders JJ, Siebes M, et al. **Intracranial blood-flow velocity and pressure measurements using an intra-arterial dual-sensor guidewire.** *AJNR Am J Neuroradiol* 2010;31:324–26
23. Schneiders JJ, Ferns SP, van Ooij P, et al. **Comparison of phase-contrast MR imaging and endovascular sonography for intracranial blood flow velocity measurements.** *AJNR Am J Neuroradiol* 2012;33:1786–90
24. Chaloupka JC, Viñuela F, Kimme-Smith C, et al. **Use of a Doppler guide wire for intravascular blood flow measurements: a validation study for potential neurologic endovascular applications.** *AJNR Am J Neuroradiol* 1994;15:509–17
25. Augsburger L, Reymond P, Rufenacht DA, et al. **Intracranial stents being modeled as a porous medium: flow simulation in stented cerebral aneurysms.** *Ann Biomed Eng* 2011;39:850–63
26. Larrabide I, Aguilar ML, Morales HG, et al. **Intra-aneurysmal pressure and flow changes induced by flow diverters: relation to aneurysm size and shape.** *AJNR Am J Neuroradiol* 2013;34:816–22
27. Shobayashi Y, Tateshima S, Kakizaki R, et al. **Intra-aneurysmal hemodynamic alterations by a self-expandable intracranial stent and flow diversion stent: high intra-aneurysmal pressure remains regardless of flow velocity reduction.** *J Neurointerv Surg* 2012 Oct 9. [Epub ahead of print]
28. Schneiders JJ, Vanbavel E, Majoie CB, et al. **A flow-diverting stent is not a pressure-diverting stent.** *AJNR Am J Neuroradiol* 2013;34:E1–4
29. Reymond P, Bohraus Y, Perren F, et al. **Validation of a patient-specific one-dimensional model of the systemic arterial tree.** *Am J Physiol Heart Circ Physiol* 2011;301:H1173–82
30. Ford MD, Alperin N, Lee SH, et al. **Characterization of volumetric flow rate waveforms in the normal internal carotid and vertebral arteries.** *Physiol Meas* 2005;26:477–88
31. Karmonik C, Yen C, Grossman RG, et al. **Intra-aneurysmal flow patterns and wall shear stresses calculated with computational flow dynamics in an anterior communicating artery aneurysm depend on knowledge of patient-specific inflow rates.** *Acta Neurochir (Wien)* 2009;151:479–85
32. Karmonik C, Yen C, Diaz O, et al. **Temporal variations of wall shear stress parameters in intracranial aneurysms—importance of patient-specific inflow waveforms for CFD calculations.** *Acta Neurochir (Wien)* 2010;152:1391–98
33. Melamed E, Lavy S, Bentin S, et al. **Reduction in regional cerebral blood flow during normal aging in man.** *Stroke* 1980;11:31–35
34. Hoi Y, Wasserman BA, Xie YJ, et al. **Characterization of volumetric flow rate waveforms at the carotid bifurcations of older adults.** *Physiol Meas* 2010;31:291–302
35. Hassan T, Ezura M, Timofeev EV, et al. **Computational simulation of therapeutic parent artery occlusion to treat giant vertebrobasilar aneurysm.** *AJNR Am J Neuroradiol* 2004;25:63–68
36. Sun Q, Groth A, Aach T. **Comprehensive validation of computational fluid dynamics simulations of in-vivo blood flow in patient-specific cerebral aneurysms.** *Med Phys* 2012;39:742–54
37. Jou LD, Quick CM, Young WL, et al. **Computational approach to quantifying hemodynamic forces in giant cerebral aneurysms.** *AJNR Am J Neuroradiol* 2003;24:1804–10
38. Boussel L, Rayz V, Martin A, et al. **Phase-contrast magnetic resonance imaging measurements in intracranial aneurysms in vivo of flow patterns, velocity fields, and wall shear stress: comparison with computational fluid dynamics.** *Magn Reson Med* 2009; 61:409–17
39. Rayz VL, Boussel L, Acevedo-Bolton G, et al. **Numerical simulations of flow in cerebral aneurysms: comparison of CFD results and in vivo MRI measurements.** *J Biomech Eng* 2008;130:051011
40. Sviri GE, Ghodke B, Britz GW, et al. **Transcranial Doppler grading criteria for basilar artery vasospasm.** *Neurosurgery* 2006;59:360–66
41. Turner CL, Higgins JN, Kirkpatrick PJ. **Assessment of transcranial color-coded duplex sonography for the surveillance of intracranial aneurysms treated with Guglielmi detachable coils.** *Neurosurgery* 2003;53:866–71
42. Ackerstaff RG, Suttorp MJ, van den Berg JC, et al. **Prediction of early cerebral outcome by transcranial Doppler monitoring in carotid bifurcation angioplasty and stenting.** *J Vasc Surg* 2005;41:618–24
43. Chang W, Landgraf B, Johnson KM, et al. **Velocity measurements in the middle cerebral arteries of healthy volunteers using 3D radial phase-contrast HYPRFlow: comparison with transcranial Doppler sonography and 2D phase-contrast MR imaging.** *AJNR Am J Neuroradiol* 2011;32:54–59
44. Cebral JR, Putman CM, Alley MT, et al. **Hemodynamics in normal cerebral arteries: qualitative comparison of 4D phase-contrast magnetic resonance and image-based computational fluid dynamics.** *J Eng Math* 2009;64:367–78
45. Waydhas C. **Intrahospital transport of critically ill patients.** *Crit Care* 1999;3:R83–89
46. Mynard JP, Wasserman BA, Steinman DA. **Errors in the estimation of wall shear stress by maximum Doppler velocity.** *Atherosclerosis* 2013;227:259–66